Automated Aerotriangulation Using Multiple Image Multipoint Matching

Peggy Agouris and Toni Schenk

Abstract

This paper deals with automating the aerotriangulation procedure using digital image processing methods and images available exclusively in digital format. A conceptual system has been developed and implemented which allows for the automatic determination of exterior orientation parameters and positions of selected points in object space using a minimal number of assumptions. In direct analogy to the preparation phase of the conventional approach, a photomosaic is automatically generated to describe the interrelationship of all photos within the available block. This photomosaic is subsequently used for the automatic extraction of approximate conjugate image coordinates.

A multiple image multipoint matching strategy has been developed to identify and precisely match conjugate points in the triple, quadruple, or multiple overlapping areas of the block. By taking into account the geometric relationship between conjugate points as expressed by their corresponding image-forming rays, and using image coordinates rather than the widely used local template coordinates, matching and block adjustment can be combined in a unique way. Thus, the mensuration and adjustment phases of classical aerotriangulation are substituted by a single digital process which allows automation of the complete procedure.

Introduction

Despite the increasing popularity of digital photogrammetry and the associated growth of research volume, aerotriangulation, one of the most important and demanding photogrammetric procedures, is still left more or less untouched by the recent trends and activities, particularly at the production level. It is the complex nature of aerotriangulation that renders its automation a rather cumbersome and challenging task, requiring the development of robust mathematical models for matching and the harmonious combination of a number of modules for its successful implementation. At the same time, it is exactly due to this complexity that human errors are often unavoidable and influence unfavorably its accuracy and overall performance. With the introduction of digital photogrammetric techniques, certain errors associated with the subjectivity of human operators during aerotriangulation may be avoided. Other potential merits as well, mainly associated with the ability to bypass dedicated photogrammetric equipment and use widely available computers instead, provide constant encouragement to all efforts towards the automation of aerotriangulation (Helava, 1989; Tsingas, 1991).

In order to successfully combine digital photogrammetry and aerotriangulation, major problems associated with the use of digital imagery and image processing techniques have to be identified and ways to overcome them need to be proposed, in order to automate several critical steps of the procedure and eventually facilitate its execution. The core of aerotriangulation is the measurement of conjugate points which in digital terms corresponds to the problem of image matching. The use of multiple images in more than one strip, with several points involved, complicates the application of existing matching techniques for aerotriangulation and, therefore, renders necessary the development of a more extensive and robust mathematical model. At the same time, the huge amount of information contained in blocks of digital images and the necessity for good approximations makes it essential to design an efficient and intelligent way to obtain a direct and reliable solution.

This paper presents a method for automated digital aerotriangulation focusing on both theoretical and implementational aspects of the issue. The objective is to perform a complete aerotriangulation procedure using digital image processing techniques and a block of imagery available solely in digital format, and automatically obtain as end products the exterior orientation parameters of photographs, conjugate points, and their object space coordinates.

Overview

Aerotriangulation is a complex procedure and, as such, it should not be expected to be performed by a single matching process but rather by a combination of single-task modules. These modules should be combined in a complete digital aerotriangulation system in a manner that would optimize the efficiency, continuity, and accuracy of the complete procedure (Agouris and Schenk, 1993). Thus, an automated aerotriangulation system should be organized in such a way that the sole input is digital imagery without any *a priori* knowledge of the exposure geometry, and all necessary approximations are derived by modules of the system itself. Restrictive and unrealistic assumptions (e.g., epipolar geometry or non-trivial approximations) have to be avoided to ensure the versatility of the procedure. A schematic overview of the proposed digital aerotriangulation procedure is presented in Figure 1. White boxes indicate processes while gray boxes correspond to results. All individual modules can be grouped into two major aerotriangulation processes, *identification* and *measurement*.

Department of Geodetic Science & Surveying, The Ohio State University, Columbus, OH 43210-1247.
P. Agouris is now with the Department of Spatial Information Science and Engineering, and the National Center for Geographic Information and Analysis, University of Maine, 5711 Boardman Hall 342, Orono, ME 04469-5711.

Photogrammetric Engineering & Remote Sensing, Vol. 62, No. 6, June 1996, pp. 703–710.

0099-1112/96/6206–703$3.00/0

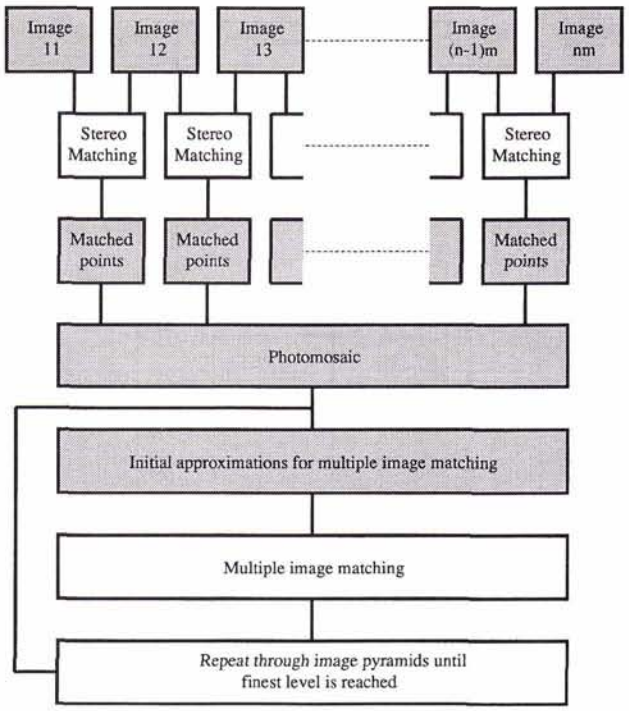

Figure 1. An overview of the presented automated aerotriangulation procedure.

Identification

The objective of the *identification* phase is to provide initial approximations which are necessary for the subsequent precise measurement of conjugate points. During the *preparation* stage of conventional aerotriangulation, an operator selects and marks conjugate pass and tie points by observing only two photographs at a time. Apart from being time-consuming, this can also lead to serious errors due to the practical inability to simultaneously observe conjugate points in multiple photographs and because of the marking procedure itself. Automated aerotriangulation, though, bypasses both problems by obtaining initial approximations of conjugate points through a photomosaic. This photomosaic can be automatically generated by estimating the approximate positions of pairs of photographs relative to each other through automatic orientation.

The automatic orientation module successfully performs the task of stereo matching. Using no initial approximations and following a combination of feature-based hierarchical matching and correlation methods with continuous updating of the results through image pyramids, conjugate points are identified in stereopairs. The reader is referred to Greenfeld and Schenk (1989) and Schenk *et al.* (1991) for a detailed description of the technique. These conjugate points provide all the necessary information for the creation of a common reference frame to which photos will later be related and which will subsequently be used to provide initial approximations for multiple image matching. A photomosaic is the realization of such a reference frame which virtually allows the evolution from stereo to *n*-stage operations. In essence, digital photomosaicking can be considered as the product of a two-step procedure combining the geometric and radiometric aspects of the problem. Initially, the position of each photo within the greater photomosaic plane has to be determined and, subsequently, it has to be filled through the proper assignment of gray values.

The geometric part is performed by a procedure similar to dependent orientation. As shown in Figure 2, the photomosaic is a digital image with a local coordinate system (x_m, y_m). For practical purposes, an identity correspondence is assumed between each point P of coordinates x_{P11}, y_{P11} in photo 11 (first strip, first photo) and its mosaic image (x_{Pm}, y_{Pm}). The two coordinate systems differ by two shifts

$$x_{Pm} = x_{P11} + dx_{11} \quad \text{and} \quad y_{Pm} = y_{P11} + dy_{11} \tag{1}$$

which are introduced simply to accomodate for deviations of the actual flight lines from ideal straight lines. These deviations would have caused some of the photos to be projected partially outside of the designated photomosaic area had the shifts not been applied.

All other photos of the block have to be correctly positioned in the photomosaic coordinate system relative to the first photo. The relationship between the (x_{ij}, y_{ij}) coordinate system of photo j in strip i and the (x_m, y_m) mosaic coordinate system can be assumed of various complexity. A projective transformation

$$x_{ij} = \frac{a_1^{ij} x_m + a_2^{ij} y_m + a_3^{ij}}{a_7^{ij} x_m + a_8^{ij} y_m + 1} \tag{2}$$

$$y_{ij} = \frac{a_4^{ij} x_m + a_5^{ij} y_m + a_6^{ij}}{a_7^{ij} x_m + a_8^{ij} y_m + 1} \tag{3}$$

is considered suitable for our purposes and offers reliable results, because it adequately describes the geometry of photomosaic generation.

The geometric solution proceeds in a successive annexation manner, which is conceptually similar to dependent orientation. The transformation parameters which precisely determine the position of the second photo in the photomosaic are determined in a least-squares solution using the conjugate points (obtained through automatic orientation) which belong to the overlapping area between the second and the first photo. In a similar way, the transformation parameters for each subsequent photo of the block are determined by tying the current image to the already existing part of the photomosaic. Once the complete set of transformation

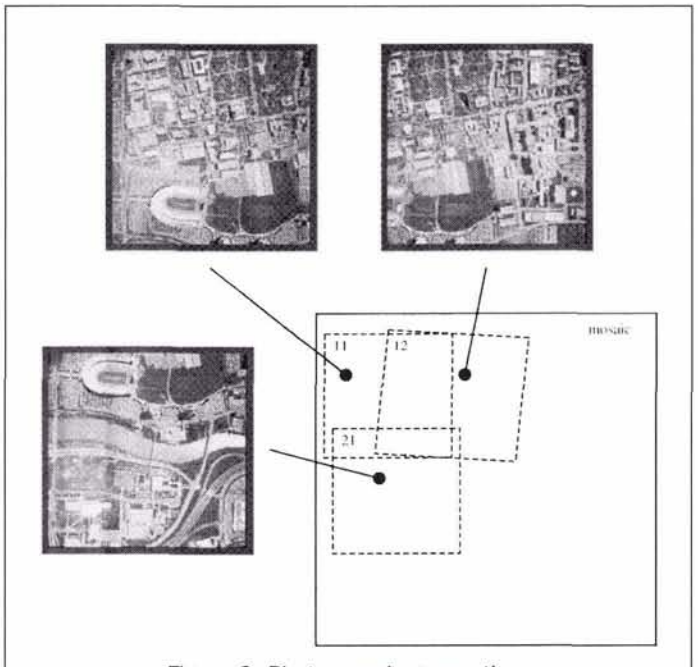

Figure 2. Photomosaic generation.

parameters for all photos has been determined (up to two parameters for the first photo and eight parameters for each additional photo), the coordinates of any photomosaic point in any photo can be determined through the inverse form of the above mentioned projective equations.

The radiometric part of photomosaicking consists of assigning gray values to each mosaic position. A mosaic pixel with coordinates (x_m, y_m) assumes the gray value of its corresponding position (x_{ij}, y_{ij}) in photo *ij*. However, in general, x_{ij} and/or y_{ij} are not integers and, therefore, there will exist two integers m and n such that

$$m \le x_{ij} < m + 1 \quad \text{and} \quad n \le y_{ij} < n + 1. \tag{4}$$

The radiometric value assignment can then be performed by any interpolation scheme. Using a bilinear interpolation in particular, the gray value assigned to the mosaic pixel (x_m, y_m) is calculated to be

$$\begin{aligned} g_m(x_m, y_m) = g_{ij}(x_{ij}, y_{ij}) &= g_{ij}(m,n)[(m+1-x_{ij})(n+1-y_{ij})] \\ &+ g_{ij}(m+1,n)[(x_{ij}-m)(n+1-y_{ij})] \\ &+ g_{ij}(m,n+1)[(m+1-x_{ij})(y_{ij}-n)] \\ &+ g_{ij}(m+1,n+1)[(x_{ij}-m)(y_{ij}-n)] \end{aligned} \tag{5}$$

where g_{ij} is the digital image function of photo *ij*. Bilinear interpolation offers excellent results in suppressing highly localized noise effects. The reader is referred to Agouris and Schenk (1993) for a detailed description of particular implementational issues of the photomosaicking module.

Once the photomosaic is available, the inverse procedure can be followed to provide the coordinates of any photomosaic point in all photos in which it might appear. Thus, we can automatically identify and distinguish the areas of double, triple, and, generally, multiple overlap within the given block. This information can be used to properly select matching candidates for the subsequent precise matching phase to ensure a strong bundle geometry. In addition, the photomosaic offers a visualization of the approximations and allows a human operator to identify and eliminate gross errors in the extraction of approximate corresponding point locations.

Measurement

The objective of the *measurement* phase is to simultaneously identify the precise position of the same object space point in two or more photos using the local gray level distributions as a measure of similarity in a multiple image matching procedure. Essentially, it is a combination of the *mensuration* and *adjustment* phases of conventional aerotriangulation in such a way that it practically allows the automation of the whole aerotriangulation procedure. The use of the well-known least-squares matching technique (Gruen, 1985) offers the advantage of having a well-defined mathematical model which permits alterations and/or expansions to accomodate certain geometric conditions. For aerotriangulation, this model has to handle multiple images. The introduction of geometric constraints expressing the relationship of conjugate image patches through their corresponding common object space area makes matching more rigorous in theory and therefore practically improved. It ensures consistent matching results and allows the combination of bundle adjustment and multiple image least-squares matching in a single procedure. The simultaneous multiphoto matching technique can be conceptually viewed as the digital equivalent of an *n*-stage comparator, allowing the measurement of conjugate points in more than two images at a time.

Multiple Image Multipoint Least-Squares Matching

By simply using the affine transformation as the geometric relationship between two or more conjugate windows according to typical least-squares matching, their complete geometric interdependence, as expressed by the satisfaction of the collinearity condition equations, is not taken into consideration. Because matching is solely based on radiometric information, windows displaying sufficient radiometric similarity can be matched even though their resulting parallax values may be unacceptable. This shortcoming can lead to erroneous matches, especially in areas of repetitive patterns, where a single window from one image displays high radiometric similarities to multiple windows of another image. This problem can be overcome either by checking the resulting parallax values or, in a more robust fashion, by introducing constraints within the geometric model used to relate conjugate patches.

Geometric constraints can be introduced either as additional equations (Gruen and Baltsavias, 1988), or by properly modifying the expression which relates the coordinate systems of corresponding windows. The image coordinates (x_p^j, y_p^j) (reduced to the principal point) of a point $P(X_p, Y_p, Z_p)$ of the object space in photo *j* satisfy the collinearity condition

$$\begin{bmatrix} x_p^j \\ y_p^j \\ -c \end{bmatrix} = \frac{1}{\lambda_p^j} \mathbf{M}_j \begin{bmatrix} X_p - X_j^0 \\ Y_p - Y_j^0 \\ Z_p - Z_j^0 \end{bmatrix} \tag{6}$$

or, in matrix notation,

$$\vec{\mathbf{x}}_p^j = \frac{1}{\lambda_p^j} \mathbf{M}_j (\vec{\mathbf{X}}_p - \vec{\mathbf{X}}_j^0) \tag{7}$$

where $\mathbf{M}_j$ is the rotation matrix of image j, $\vec{\mathbf{X}}_j^0$ are the the ground coordinates of the exposure center of photo *j*, and λ_p^j is the associated scale factor.

Backsolving the collinearity condition for the image of the same point P in photo *i*, we obtain

$$\vec{\mathbf{X}}_p = \lambda_p^i \mathbf{M}_i^T \vec{\mathbf{x}}_p^i + \vec{\mathbf{X}}_i^0 \tag{8}$$

and substituting this expression of $\vec{\mathbf{X}}_p$ into Equation 7 gives

$$\vec{\mathbf{x}}_p^j = \frac{\lambda_p^i}{\lambda_p^j} \mathbf{M}_j \mathbf{M}_i^T \vec{\mathbf{x}}_p^i + \frac{1}{\lambda_p^j} \mathbf{M}_j (\vec{\mathbf{X}}_i^0 - \vec{\mathbf{X}}_j^0) \tag{9}$$

which can also be written as a set of three equations

$$x_p^j = \frac{1}{\lambda_p^j} [m_j^{11}\ m_j^{12}\ m_j^{13}] (\lambda_p^i \mathbf{M}_i^T \vec{\mathbf{x}}_p^i + \vec{\mathbf{X}}_i^0 - \vec{\mathbf{X}}_j^0) \tag{10}$$

$$y_p^j = \frac{1}{\lambda_p^j} [m_j^{21}\ m_j^{22}\ m_j^{23}] (\lambda_p^i \mathbf{M}_i^T \vec{\mathbf{x}}_p^i + \vec{\mathbf{X}}_i^0 - \vec{\mathbf{X}}_j^0) \tag{11}$$

$$-c = \frac{1}{\lambda_p^j} [m_j^{31}\ m_j^{32}\ m_j^{33}] (\lambda_p^i \mathbf{M}_i^T \vec{\mathbf{x}}_p^i + \vec{\mathbf{X}}_i^0 - \vec{\mathbf{X}}_j^0) \tag{12}$$

By dividing the first two equations by the third one, we obtain a set of two equations

$$x_p^j = \frac{-c\ [m_j^{11}\ m_j^{12}\ m_j^{13}] (\lambda_p^i \mathbf{M}_i^T \vec{\mathbf{x}}_p^i + \vec{\mathbf{X}}_i^0 - \vec{\mathbf{X}}_j^0)}{[m_j^{31}\ m_j^{32}\ m_j^{33}] (\lambda_p^i \mathbf{M}_i^T \vec{\mathbf{x}}_p^i + \vec{\mathbf{X}}_i^0 - \vec{\mathbf{X}}_j^0)} \tag{13}$$

$$y_p^j = \frac{-c\ [m_j^{21}\ m_j^{22}\ m_j^{23}] (\lambda_p^i \mathbf{M}_i^T \vec{\mathbf{x}}_p^i + \vec{\mathbf{X}}_i^0 - \vec{\mathbf{X}}_j^0)}{[m_j^{31}\ m_j^{32}\ m_j^{33}] (\lambda_p^i \mathbf{M}_i^T \vec{\mathbf{x}}_p^i + \vec{\mathbf{X}}_i^0 - \vec{\mathbf{X}}_j^0)} \tag{14}$$

where m_j^{mn} is the element in the m^{th} row and n^{th} column of the rotation matrix $\mathbf{M}_j$ of image *j*. The above expressions relate the (x_p^j, y_p^j) image coordinates of point P in photo *j* to the (x_p^i, y_p^i) image coordinates of the same point in photo *i* as a

function of the exterior orientation parameters of both photos and the scale factor of P in one of them. For a fixed point P (x_P^i, y_P^i) in photo i, the coordinates (x_P^j, y_P^j) of its conjugate position in photo j will change if and only if certain exterior orientation elements of either image and/or the scale factor λ_P^i change. For an image i, fixed in the object space, the scale factor λ_P^i uniquely defines the survey coordinates (X_P, Y_P, Z_P) and, consequently, the position of point P in the object space from its fixed coordinates in the same photo as

$$X_P = \lambda_P^i [m_i^{11} x_P^i + m_i^{21} y_P^i + m_i^{31}(-c)] + X_i^0 \quad (15)$$

$$Y_P = \lambda_P^i [m_i^{12} x_P^i + m_i^{22} y_P^i + m_i^{32}(-c)] + Y_i^0 \quad (16)$$

$$Z_P = \lambda_P^i [m_i^{13} x_P^i + m_i^{23} y_P^i + m_i^{32}(-c)] + Z_i^0 \quad (17)$$

The fixed image of point P in image i is defining a ray, connecting the exposure station of image i, the image of P in photo i, and the object space point P. The position of that ray in object space is defined by the exterior orientation parameters of photo i. On the same ray, the position of P in the object space is defined by the scale factor λ_P^i. The coordinates of P in another image j are defined from the point's object space position and the exterior orientation parameters of that image. Equations 13 and 14 express this relationship for a pair of images and a single point. A similar set of equations can be formed for every other object space point appearing in photos i and j. Each new point Q introduces a new scale factor λ_Q^i, while points in the same image are related by a common set of exterior orientation parameters. For sufficiently small image patches which do not present abrupt height variations in the object space, all points within a patch can be reasonably assumed to have the same scale factor. A set of equations can thus be formed, relating the image coordinates of a patch in image j to its conjugate patch in image i through the exterior orientation parameters of both photos and a scale factor, instead of the traditionally used affine transformation.

Conceptually, by applying Equations 13 and 14 to the coordinates of conjugate window pairs (w_i, w_j) and dropping the index P, we have

$$(x_j, y_j) = \phi^{ij} (x_i, y_i) \quad (18)$$

with ϕ being the function described by Equations 13 and 14. This function expresses the relationship between a pair of windows through a common reference which, in this case, is the object space patch.

When initial approximations (obtained through the photomosaic) are available in the form of conjugate points in a block, approximations for the exterior orientation parameters of each image as well as for the object space coordinates of points can be determined through a typical block adjustment procedure. These initial approximations will then be refined through a multipoint multiple image matching adjustment. Using the initial rough approximations, new approximate conjugate positions for a stationary patch centered at pixel (x_i, y_i) of image i can be found in all other images. If the original approximations were perfect, these conjugate patches would display (after a radiometric histogram equalization) similar gray values. Differences in gray values between patch $g_i(x_i, y_i)$ and its approximate conjugate position in photo j, $g_j(x_j^0, y_j^0)$, are due to the fact that the two patches are not exactly conjugate. The coordinates of $g_j(x_j, y_j)$ have to be properly updated to become truly conjugate to $g_i(x_i, y_i)$. This will be achieved by updating the exterior orientation parameters of photos i and j and the scale factor λ_i in such a way that the gray value differences between conjugate patches will be minimized.

By using the n_1 by n_2 pixel patch in photo i as a template, a total of $n_1 \cdot n_2$ observation equations can be written to compare it to its conjugate patch in photo j. They are linearized as

$$g_i(x_i, y_i) - e(x_i, y_i, x_j, y_j) = g_j^0(x_j^0, y_j^0) + g_{jx}\, dx_j + g_{jy}\, dy_j \quad (19)$$

which becomes

$$\begin{aligned} g_i(x_i, y_i) - e(x_i, y_i, x_j, y_j) = {} & g_j^0(x_j^0, y_j^0) \\ & + g_{jx} \frac{\partial x_j}{\partial o_1^j} do_1^j + \ldots + g_{jy} \frac{\partial y_j}{\partial o_m^j} do_m^j \\ & + g_{jx} \frac{\partial x_j}{\partial o_1^j} do_1^j + \ldots + g_{jy} \frac{\partial y_j}{\partial o_m^j} do_m^j \\ & + g_{jx} \frac{\partial x_j}{\partial \lambda_i^P} d\lambda_i^P + g_{jy} \frac{\partial y_j}{\partial \lambda_i^P} d\lambda_i^P \end{aligned} \quad (20)$$

and

$$\begin{aligned} g_i(x_i, y_i) - e(x_i, y_i, x_j, y_j) = {} & g_j^0(x_j^0, y_j^0) + [g_{jx} \frac{\partial x_j}{\partial o_1^j} + g_{jy} \frac{\partial y_j}{\partial o_1^j}]\, do_1^j \\ & + \ldots + [g_{jx} \frac{\partial x_j}{\partial o_m^j} + g_{jy} \frac{\partial y_j}{\partial o_m^j}]\, do_m^j \\ & + [g_{jx} \frac{\partial x_j}{\partial \lambda_i^P} + g_{jy} \frac{\partial y_j}{\partial \lambda_i^P}]\, d\lambda_i^P \end{aligned} \quad (21)$$

where λ_i^P is the scale factor for the patch centered in point P in photo i, and $(o_1^i, \ldots, o_m^i)$, $(o_1^j, \ldots, o_m^j)$ are any preselected set of m orientation parameters for photos i and j, respectively. In the most general case, all exterior orientation parameters of each photo are considered adjustable; thus, $m = 6$ and

$$[o_1^i, o_2^i, o_3^i, o_4^i, o_5^i, o_6^i]^T = [\omega^i, \phi^i, \kappa^i, X_0^i, Y_0^i, Z_0^i]^T \quad (22)$$

The design matrix **A** for least-squares matching will include the derivatives of all observation equations with respect to all unknowns. Each line of the **A** matrix will include 12 nonzero elements at the positions corresponding to the exterior orientation parameters of the two photos on which the conjugate patches (one of which is always the template) appear, as well as one nonzero element corresponding to the scale factor of the specific template. The pattern of the **A** matrix, assuming the exterior orientation elements to be ordered first and the scale factors grouped as the last elements of the matrix of the unknowns, is shown in Figure 3. The figure illustrates an example case of a total of

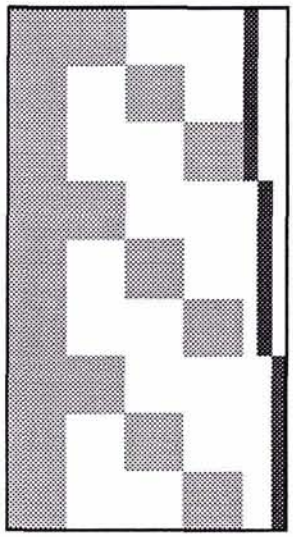

Figure 3. Sparsity pattern of the design matrix for multiple image multipoint least-squares matching with geometric constraints.

three points appearing in the overlapping area of four images, using the patches in image 1 as reference templates. Light gray boxes indicate derivatives with respect to the exterior orientation parameters, while dark gray boxes correspond to derivatives with respect to the scale factors. For patches of n_1 by n_2 pixels, the dimensions of light gray boxes are $(n_1 \cdot n_2)$ by 6, while each corresponding dark box includes $(n_1 \cdot n_2)$ by 1 elements. In general, assuming a total of n photos and m distinct patches or corresponding points, there exists a total of $(6 \cdot n) + m$ unknowns

$$\mathbf{X}^{\mathrm{T}} = [do_1^1,\ do_2^1,\ \ldots,\ do_6^n,\ d\lambda_1,\ \ldots\ d\lambda_m]^{\mathrm{T}}. \tag{23}$$

The least-squares solution is obtained as

$$\hat{\mathbf{X}} = (\mathbf{A}^{\mathrm{T}}\ \mathbf{P}\ \mathbf{A})^{-1}\ \mathbf{A}^{\mathrm{T}}\ \mathbf{P}\ \mathbf{L} \tag{24}$$

with the k^{th} element of the observation vector $\mathbf{L}$ including the comparison of the corresponding gray values of a patch in image j to its template in image i: i.e.,

$$\mathbf{L}_k = g_i\ (x_i,\ y_i) - g_j^0\ (x_j^0,\ y_j^0). \tag{25}$$

The residual vector for the gray value observations will be

$$\mathbf{V} = \mathbf{A}\hat{\mathbf{X}} - \mathbf{L} \tag{26}$$

and the estimated variance of unit weight

$$\hat{\sigma}_o^2 = \frac{\mathbf{V}^{\mathrm{T}}\ \mathbf{P}\ \mathbf{V}}{df} \tag{27}$$

where df denotes the degree of freedom, equal to the number of equations minus the number of unknowns. The number of equations, and, equivalently, the dimension of the $\mathbf{L}$ vector, depends on the number of formed pairs of conjugate patches. Assuming p pairs and patches of n_1 by n_2 pixels, a total of $p \cdot n_1 \cdot n_2$ equations will be formed.

Because the original model is non-linear, the final solution is obtained through iterations. After each iteration, the image coordinates of point P in photo j are updated due to corrections in orientation parameters as

$$\begin{aligned} x_j = x_j^0 &+ \frac{\partial x_j}{\partial o_1^j}\,\hat{do}_1^j + \ldots + \frac{\partial x_j}{\partial o_m^j}\,\hat{do}_m^j \\ &+ \frac{\partial x_j}{\partial o_1^i}\,\hat{do}_1^i + \ldots + \frac{\partial x_j}{\partial o_m^j}\,\hat{do}_m^j + \frac{\partial x_j}{\partial \lambda_i^p}\,\hat{d\lambda}_i^p \end{aligned} \tag{28}$$

and

$$\begin{aligned} y_j = y_j^0 &+ \frac{\partial y_j}{\partial o_1^j}\,\hat{do}_1^j + \ldots + \frac{\partial y_j}{\partial o_m^j}\,\hat{do}_m^j \\ &+ \frac{\partial y_j}{\partial o_1^j}\,\hat{do}_1^i + \ldots + \frac{\partial y_j}{\partial o_m^j}\,\hat{do}_m^j + \frac{\partial y_j}{\partial \lambda_i^p}\,\hat{d\lambda}_i^p \end{aligned} \tag{29}$$

For these new coordinates, new gray values are determined from the original image function through a bilinear interpolation, and the observations vector is properly updated. The $(x_i,\ y_i)$ coordinates of the reference template obviously remain constant throughout the adjustment procedure.

Assuming, for example, image patches of 5 by 5 pixels, each pair of conjugate patches produces a total of 25 observation equations with 13 unknowns, i.e., six exterior orientation parameters for each image and one scale factor. By using the same patch size and number of unknowns for a patch in the common overlapping area of n photographs, a total of $25 \cdot (n - 1)$ observation equations with $(6 \cdot n) + 1$ unknowns are formed through comparison to the reference template. Despite the fact that, for every $n \geq 2$ (which would be the case even for a single pair of corresponding patches) we have more equations than unknowns, a bundle solution obviously cannot be obtained. The poor geometry, due to narrow rays formed by the small patch size, will lead to an ill-conditioned system and, therefore, to highly unreliable results. In order to overcome this problem, the patches should follow a distribution similar to that of pass and tie points in a typical block adjustment (i.e., corresponding to the Von Gruber points). Even though a pair of patches produces in this example 25 equations, each patch is essentially expected to contribute to the geometric part of the adjustment information corresponding to that provided by a single point in a traditional block adjustment. By using an adequate number of properly distributed patches, sufficient geometric information becomes available to successfully tie all photos in a block.

To eliminate the datum defect problem, control points have to be used or certain parameters have to be considered constant. The datum defect for a block adjustment is seven, expressing the three translations, three rotations, and one scale factor that relate two three-dimensional systems. It can be eliminated by using one height and two full control points. Alternatively, by keeping the six exterior orientation parameters of an image and the one scale factor of a patch constant, seven independent pieces of information can be provided, thus permitting a minimum constraint solution. This solution would be geometrically considered as the block equivalent of a dependent orientation, whereby one photo is moved and rotated with respect to a fixed one in order for a model to be formed.

In general, if *a priori* stochastic information for any unknown parameters is available (e.g., obtained by a GPS receiver in the airplane (Lucas, 1987)), it can be introduced into the adjustment procedure as additional observation equations of the form

$$L_{ij}^e = o_j^{i\alpha} - o_j^{io} = v_{o_j} - do_j \tag{30}$$

$$L_i^{\lambda} = \lambda_i^{\alpha} - \lambda_i^{o} = v_{\lambda_i} - d\lambda_i \tag{31}$$

in a manner similar to the introduction of observations of exterior orientation parameters or survey coordinates into a block adjustment (Merchant, 1984). The superscripts α and o are used to denote the adjusted and current approximate values, respectively. Assuming a weight matrix $\mathbf{P}^e$ associated with the additional observations on exterior orientation elements, and $\mathbf{P}^{\lambda}$ the corresponding weight matrix for scale factors, the introduction of these additional observations will alter the solution as

$$\begin{bmatrix} \hat{\mathbf{X}}^e \\ \hat{\mathbf{X}}^{\lambda} \end{bmatrix} = \begin{bmatrix} \mathbf{A}^{e\mathrm{T}}\ \mathbf{P}\ \mathbf{A}^e + \mathbf{P}^e & \mathbf{A}^{e\mathrm{T}}\ \mathbf{P}\ \mathbf{A}^{\lambda} \\ \mathbf{A}^{\lambda\mathrm{T}}\ \mathbf{P}\ \mathbf{A}^e & \mathbf{A}^{\lambda\mathrm{T}}\ \mathbf{P}\ \mathbf{A}^{\lambda} + \mathbf{P}^{\lambda} \end{bmatrix}^{-1} \begin{bmatrix} \mathbf{A}^{e\mathrm{T}}\ \mathbf{P}\ \mathbf{L} - \mathbf{P}^e\ \mathbf{L}^e \\ \mathbf{A}^{\lambda\mathrm{T}}\ \mathbf{P}\ \mathbf{L} - \mathbf{P}^{\lambda}\ \mathbf{L}^{\lambda} \end{bmatrix} \tag{32}$$

where $\mathbf{A}^e$ is that part of the matrix $\mathbf{A}$ referring to exterior orientation parameters and $\mathbf{A}^{\lambda}$ is the part referring to the scale factors. In comparison, the direct solution (Equation 24) can be expressed, using the above submatrices, as

$$\begin{bmatrix} \hat{\mathbf{X}}^e \\ \hat{\mathbf{X}}^{\lambda} \end{bmatrix} = \begin{bmatrix} \mathbf{A}^{e\mathrm{T}}\ \mathbf{P}\ \mathbf{A}^e & \mathbf{A}^{e\mathrm{T}}\ \mathbf{P}\ \mathbf{A}^{\lambda} \\ \mathbf{A}^{\lambda\mathrm{T}}\ \mathbf{P}\ \mathbf{A}^e & \mathbf{A}^{\lambda\mathrm{T}}\ \mathbf{P}\ \mathbf{A}^{\lambda} \end{bmatrix}^{-1} \begin{bmatrix} \mathbf{A}^{e\mathrm{T}}\ \mathbf{P}\ \mathbf{L} \\ \mathbf{A}^{\lambda\mathrm{T}}\ \mathbf{P}\ \mathbf{L} \end{bmatrix} \tag{33}$$

By performing multiple image multipoint matching as presented in this section, we inherently ensure that conjugate image rays intersect at a point in the object space, as well as explore the interrelationship of various patches in the same image. The use of object space constraints to express the relationship of two or more conjugate windows allows the combination of radiometric and geometric solutions into a

Figure 4. The digital photomosaic.

single adjustment procedure. Thus, block adjustment and least-squares matching can be combined, allowing the solution of matching ambiguities and producing a geometrically coherent solution.

Summarizing, the presented automated aerotriangulation strategy proceeds as follows:

- A photomosaic of the given block is automatically generated through successive use of the automatic orientation module between stereopairs.
- Points are selected (manually or automatically) in the overlapping regions of the photomosaic. The distribution of these points must be such that a robust block adjustment solution is feasible.
- Approximate values for the location of these points in each block image are obtained from Equations 2 and 3.
- From the resulting image coordinates, an initial block adjustment is performed to provide the necessary approximations for the exterior orientation parameters of each image and the object space coordinates of each point.
- For every object space point, its image in one photograph is selected to be the matching template. The selection can be based on various principles. For example, one can select the image of the point in the leftmost photo of the uppermost strip, or select as matching template the image which offers highest radiometric variations (highest entropy value). The latter option offers the potential to optimize matching accuracies.
- Once a template is selected, approximations for the corresponding scale factor are calculated from the current values of exterior orientation parameters and the approximate object space coordinates. From this information, initial approximations of conjugate image windows are defined.
- Finally, multiple image multipoint matching is performed. During this adjustment, for every object space point, its images in all photos are compared to its template pairwise. From the adjustment, exterior orientation parameters and scale factors are updated. Through their update, the image coordinates of conjugate patches are also updated, new observation equations are formed, and a new iteration is performed. Iterations stop when the parameters do not change significantly.

The procedure offers as end products the exterior orientation parameters of each photo of the block, the object space coordinates of the selected points, and their conjugate locations in multiple images.

Experiments

To implement and study the previously described automatic aerotriangulation procedure, a block of digital images was used. It contained eight photos arranged in two strips of four photos each, depicting the broader area of the campus of The Ohio State University at a scale of 1:4000. The overlap was 60 percent within a strip (endlap) and 35 percent between strips (sidelap).

Following the previously described procedure, the eight photos were combined in a photomosaic (Figure 4). The number of matched points per stereopair was on the average 120 for models along strips, and 65 for models formed between strips. The difference in the number of matched points for these two cases is of course expected, due to their difference in overlap.

The accuracy of the photomosaic expresses how close to true conjugate points are the approximations derived from it. This information is valuable for subsequent precise matching because it affects the window size selection. Windows have to be large enough to ensure sufficient similarity between approximate conjugate windows, but at the same time they have to be kept relatively small to avoid unnecessary computational burdens. The pixel size, changing in various levels of image pyramids, can be used to transform absolute measures of accuracy (μm) into relative indices (pixels). According to the desirable window size and the accuracy of the available approximations, an image resolution is chosen that ensures sufficiently overlapping windows. On this resolution level, multiple image matching is performed, and the results serve as initial approximations for matching in finer resolutions, until the finest resolution is reached and the most accurate solution is obtained.

To assess the photomosaic accuracy, a total of 60 test points approximating a regular 6 by 10 grid were selected. Using the (x_m, y_m) photomosaic coordinates of these points and the computed projective transformation parameters $a_1^{ij}, \ldots a_8^{ij}$, the (x_{ij}^a, y_{ij}^a) coordinates of each point in photo ij were automatically calculated. Subsequently, each test point was manually identified in every photo in which it appeared and its coordinates (x_{ij}^m, y_{ij}^m) were recorded. These manually collected coordinates were considered as the "true" ones to which the automatically determined coordinates were compared for a definite measure of the accuracy of the photomosaic. Figure 5 shows the radial distance δr, defined as

$$\delta r = \sqrt{(x_{ij}^m - x_{ij}^a)^2 + (y_{ij}^m - y_{ij}^a)^2} \qquad (34)$$

between manually and automatically detected test points. It can be seen that approximately 81 percent of the test points deviate radially by no more than 2.8 pixels from the manually determined ones. This radial distance corresponds to deviations of up to two pixels in both x and y directions, which, for the current resolution of the digital images (1024 by 1024 pixels representing an analog image of 23 by 23

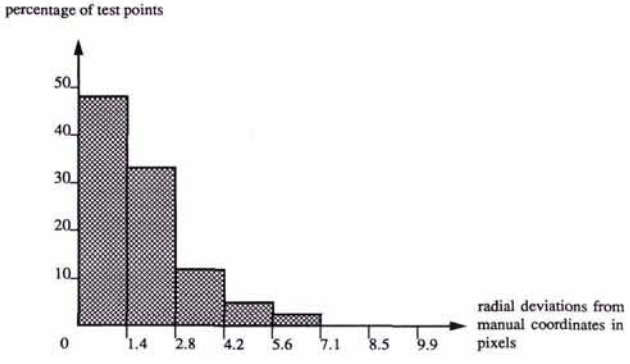

Figure 5. Photomosaic accuracy using projective transformation.

cm^2), is equivalent to approximately 500 μm. The results slightly deteriorate towards the end of each strip in a manner similar to error propagation during strip formation in a photogrammetric plotter. By adding photos to a photomosaic already created by the previous members of a strip, a leveling-type error is introduced, with error magnitudes increasing along strips due to error propagation. For this application, with only four photos per strip, the deterioration is rather insignificant, but it could be quite important when longer strips are used. In that case, control points further along the strip should be used to limit the associated distortions.

The above results show that the photomosaic can be succesfully used to automatically obtain first approximations of conjugate locations for the subsequent precise multiphoto matching. These approximations will serve as centers of windows which overlap sufficiently, ensuring a successful least-squares matching solution as previously discussed. Even for small windows of 5 by 5 pixels, the radial deviation of 2.8 pixels ensures a minimum overlap of 36 percent in area or 50 percent in each direction between conjugate windows. The larger coordinate deviations (5.6 pixels) were observed in positions of extreme relief displacements (very high buildings). This is rather expected because the theoretical model of projective transformation expresses the three-dimensional relationship of two planes. If the projective transformation parameters relating each photo to the photomosaic are properly determined from precise (subpixel accuracy) stereomatching, the accuracy of the photomosaic will solely depend on how well the terrain resembles a plane. Nearly flat terrains offer higher accuracies, while severe height variations lower the accuracy. It should be mentioned that points matched through the automatic orientation module are mainly located on the ground (Stefanidis *et al.*, 1991). Matched points on high buildings are very scarce because their parallax values very often exceed the acceptable range. Therefore, the mosaic determined using conjugate points obtained through automatic orientation best relates the planes defined by the ground surface depicted in the photos, rather than by buildings and other height extremities.

Prior to matching, a radiometric correction was performed to minimize gray value scale and variance differences between conjugate image patches. Gross variations in exposure conditions were corrected by performing a linear histogram scaling procedure. That way, radiometric differences in scale and standard deviation are minimized before the actual matching process itself accomodates for the remaining differences through corrections of exterior orientation parameters and the position of the points in object space.

Using the photomosaic as a common reference frame, a total of 27 points were identified in the block of eight photos. They were selected in a way that would provide sufficient coverage of multiple overlapping areas, allowing a geometrically strong block adjustment solution, while at the same time making sure that the resulting windows are rich in radiometric content. Using the projective transformation parameters and the photomosaic coordinates of the 27 points, the coordinates of every point in each photo were calculated. The approximate image coordinates determined through the photomosaic were examined manually to ensure that no blunders existed among them. These coordinates are then used to obtain approximate exterior orientation and object space coordinate values, as discussed in the previous section.

For precise matching, the size of the windows is kept small, e.g., 5 by 5 or 7 by 7 pixels, or even higher when radiometric variations within the resulting windows are considered inadequate. Small window sizes ease computational burden and ensure satisfaction of the geometric assumptions inherent in the geometric model (i.e., common scale factor for all pixels of a patch) used to relate conjugate windows. For every object space point, the corresponding window in one of the photos in which it is imaged is kept stable and serves as the matching template. The approximate values of the exterior orientation parameters of each photo and the scale coefficient of the template are then used to determine the conjugate positions of each pixel of the template in all photos in which it may appear. First approximations of the conjugate windows are defined in this manner. It is obvious that windows other than the template will most likely not correspond to integer pixel locations. Thus, gray value interpolation is required, even from the stage of initial approximations. This procedure is repeated for each of the processed object space points to produce the necessary input for the subsequent stage of precise matching.

Multiple image multipoint matching was then performed using 1024- by 1024-pixel digitized versions of the photos. To eliminate the datum defect, the exterior orientation parameters of one photograph (photo one in strip one) and the scale factor of one point in this photo were kept constant, and their values remained unchanged during the adjustment. The results of this solution were subsequently used as approximations for repeating matching in a finer resolution level (2048 by 2048). There, the final solution comprised of exterior orientation parameters and scale factors was obtained.

To examine the accuracy of the obtained conjugate points, an even finer version of the images (4096 by 4096 pixels) was used. The coordinates from both 1024 by 1024 and 2048 by 2048 levels were transfered to that finer level where they were manually compared to their respective "true" conjugate positions. Thus, subpixel measures of accuracy were estimated. The operator's observations are reasonably assumed to be as accurate as 0.5 pixel at the resolution level where the image is directly observed. The deviations of matched points from true conjugate locations were determined for each set of conjugate points. Points matched at the 1024 by 1024 pixel level presented an average deviation from "true" conjugate location on the order of 1.3 pixels at the 4096 by 4096 resolution level, which corresponds to an accuracy of almost 0.325 of a pixel at the level where matching was actually performed (1024 by 1024, in this case). Points matched at the 2048 by 2048 resolution level presented an average deviation of 0.6 pixel in 4096- by 4096-pixel imagery, which corresponds to 0.3 of a pixel at the level where matching was performed (2048 by 2048).

It is important to realize that the accuracy of determining conjugate points is a representative measure of the performance of the technique, because they are calculated by taking into account all the elements determined by multiple image multipoint least-squares matching (exterior orientation, scale factors). The presented matching results indicate sufficient accuracies to support the presented digital aerotriangulation strategy.

Concluding Remarks

The present paper deals with performing an automated aerotriangulation using digital image processing methods and images available exclusively in digital format. A conceptual system has been developed and implemented which allows the determination of exterior orientation parameters and positions of selected points in object space using a minimal number of assumptions.

Initial experimental results confirmed the derived theoretical strategy and support its quality and feasibility. The introduction of digital techniques offers a solution to the problem of subjective point identification errors associated with a human operator who is unable to observe more than

two photos at a time. Instead, multiphoto matching offers essentially a digitally implemented *n*-stage comparator. Having this as its core module, the presented automated digital aerotriangulation scheme becomes flexible and efficient.

The potential to bypass expensive and dedicated equipment (e.g., analytical plotters) and personnel by performing the necessary operations in a computer may revolutionize aerotriangulation. Not only could it change the way aerotriangulation is currently carried out, but it would mainly boost its practicality and application in scientific fields and communities (e.g., architecture, industry, and medicine) which are currently hesitant or turned off by the aforementioned equipment and personnel requirements.

References

Agouris, P., 1992. *Multiple Image Multipoint Matching for Automatic Aerotriangulation*, Ph.D. Dissertation, Department of Geodetic Science & Surveying, The Ohio State University, Columbus, Ohio.

Agouris, P., and A.F. Schenk, 1993. Automatic Processing of Image Blocks, *Proceedings 1993 ASPRS Annual Convention*, New Orleans, 3:11–20.

Greenfeld, J.S., and A.F. Schenk, 1989. Experiments with Edge–Based Stereo Matching, *Photogrammetric Engineering & Remote Sensing*, 55(12):1771–1777.

Gruen, A., 1985. Adaptive Least Squares Correlation: A Powerful Image Matching Technique, *South African Journal of Photogrammetry, Remote Sensing and Cartography*, 14(3):175–187.

Gruen, A., and E.P. Baltsavias, 1988. Geometrically Constrained Multiphoto Matching, *Photogrammetric Engineering & Remote Sensing*, 54(5):633–641.

Helava, U.V., 1989. Digital Comparator Correlator System (DCCS), *ISPRS Journal of Photogrammetry & Remote Sensing*, 44(1):37–47.

Lucas, J.R., 1987. Aerotriangulation without Ground Control, *Photogrammetric Engineering & Remote Sensing*, 53(3):311–314.

Merchant, D.C., 1984. *Analytical Photogrammetry, Theory and Practice*, Lecture Notes, Department of Geodetic Science & Surveying, The Ohio State University, Columbus, Ohio.

Schenk, A.F., J.C. Li, and C. Toth, 1991. Towards an Autonomous System for Orienting Digital Stereopairs, *Photogrammetric Engineering & Remote Sensing*, 57(8):1057–1064.

Stefanidis, A., P. Agouris, and A.F. Schenk, 1991. Aspects of Accuracy in Automatic Orientation, *Proceedings 1991 ASPRS Annual Convention*, Baltimore, 5:334–343.

Tsingas, V., 1991. Automatische Aerotriangulation, *Proceedings 43rd Photogrammetric Week*, Institute for Photogrammetry, Stuttgart University, 15:253–268.

PE&RS Appoints New Associate Editor and Update Editor

Dr. Peggy Agouris has agreed to serve as the Associate Editor for Softcopy Photogrammetry in *Photogrammetric Engineering and Remote Sensing*. Agouris is assistant professor at the University of Maine, Department of Spatial Information Science and Engineering, and a senior researcher at the National Center for Geographic Information and Analysis. She has a master's and doctoral degree in softcopy photogrammetry from the Department of Geodetic Science and Surveying at The Ohio State University in Columbus, Ohio. Before going to the University of Maine, Agouris was the senior scientific associate at the Institute of Geodesy and Photogrammetry, Swiss Federal Institute of Technology in Zurich, Switzerland.

Dr. Tony Stefanidis, also at the University of Maine, will be the new update editor for the Softcopy Photogrammetry column.

All manuscripts should be sent to ASPRS at 5410 Grosvenor Lane, Suite 210, Bethesda, Maryland 20814. To contact Dr. Agouris, call 207-581-2127 or e-mail peggy@spatial.maine.edu .